“This is an Accepted Manuscript of an article published by Taylor & Francis in International Journal of Architectural Heritage, 8:5, 627-648, published online: 11 Feb 2014, available at: https://doi.org/10.1080/15583058.2012.704480.”

Textile Reinforced Mortar as strengthening material for masonry arches

L. Garmendia[a], J.T. San-José[b], P. Larrinaga[a], D. García[a]

[a]*TECNALIA, c/Geldo, Parque Tecnológico de Bizkaia, Ed. 700, 48160, Derio, Spain*

[b]*Dept. of Engineering in Mining, Metallurgy and Science of Materials (UPV/EHU). c/Alda, Urquijo s/n, 48013 Bilbao, Spain*

leire.garmendia@tecnalia.com

The Strengthening of Masonry Arches with Textile-Reinforced Mortar

Masonry arches are an important part of our built heritage that we need to preserve. Research and advanced studies of historical masonry structures have progressed slowly in comparison to studies on structures made of other materials (concrete, steel, etc.), due to which there is a lack of knowledge and experience in this field. This research evaluates the effectiveness of Basalt Textile Reinforced Mortar (BTRM) as a compatible strengthening composite material for stone masonry arches, providing researchers with further quantitative data. To do so, eleven masonry arches were constructed, strengthened with different layouts and tested. Furthermore, the BTRM was characterised by testing its constituent materials and the composite material. Once analysed and compared with other studies, the results showed that BTRM is a promising solution for strengthening stone masonry arches. It is easy to apply, compatible and gives the original structures greater mechanical properties, in terms of ultimate load and deformation capacity.

Keywords: masonry, arch, strengthening, composites, TRM

1. Introduction

Masonry arches are part of our built heritage, a fact which people tend to ignore, perhaps because of the frequency with which we use them. Among other structures, they form part of buildings, tunnels and bridges, making it virtually impossible to calculate their overall numbers. A relevant piece of information is that in 1998, a total of 22,827 parish churches were recorded on the national census in Spain. In the case of railways, the International Union of Railways (UIC) reported the following numbers of arches and culverts: in France (78,000 – 76.8% of total bridge stock), Italy (56,888 – 94.5%), Germany (35,000 – 38.9%), India (20,967 – 18%), UK (17867 – 46.9%), and Portugal (11,746 – 89.8%), Czech (4,858 – 18.9%) (Orban, 2007). In Spain, according to the general bridge inventory, masonry arch bridges constitute 45% of the total number of railway bridges (Jerez et al., 2007).

The UIC states that 70% of these masonry structures are between 100 and 150 years old and there is also a significant proportion (approx. 12%) of bridges over 150 years old. Moreover, an important proportion (15%) is in poor or very poor condition (Orban, 2007).

Even though masonry arches are solid structures, time has taught us that environmental conditions (Herrera et al., 2009) and the loads these structures carry (usage and accidents) can lead to their collapse (Zonta et al., 2008; Oliveira et al., 2010), which leaves much of our architectonic and cultural heritage at risk (Figure 1).

Currently, new approaches are being developed to retrofit masonry arches based on innovative reinforcement systems which are currently known as "composites". In the 80s, new reinforcement materials presented in the form of Fibre-Reinforced Polymers (FRP), which are synthetic fibres embedded in resins, were introduced to the world of masonry restoration (Croci et al., 1987). Unlike traditional reinforcement systems, FRP is a lightweight material with high specific tensile strength and rigidity and its good resistance to corrosion along with other durable properties means that it requires little maintenance. Over recent years, experimental works have demonstrated that it is a valid option for the strengthening and/or repair of masonry (Seible, 1995; Triantafillou, 1996) and, particularly, arched masonry structures (Foraboschi, 2001; Lissel and Gayevoy, 2003; Oliveira et al., 2006, Cancelliere et al. 2010).

Despite the advantages of using FRP, it is worth mentioning the following disadvantages: it is a fragile material, it cannot be applied over humid substrates, it must be used within a narrow temperature range, it is not fire-resistant, it is often incompatible with the parent material (permeability, etc.), it has a high unit cost and its long-term durability requires further investigation. Moreover, its application to masonry structures is complex; epoxi resins create a barrier which prevents thermohygrometric transfer between the structure and the outside, hence the moisture remains trapped within the structure and cannot migrate naturally towards the outside. To ensure adequate masonry permeability and comply with restoration requirements (cultural and technical compatibility), most of the boundary areas must be left without reinforcement (Foraboschi, 2004).

One alternative to bypass the drawbacks associated with these physico-chemical incompatibilities (water-vapour permeability) is the replacement of epoxy resin with an inorganic mortar. Furthermore, in order to guarantee good matrix-core adhesion, fibres may be replaced by grid textiles. This composite material based on textiles embedded in a mortar matrix is known as Textile Reinforced Mortar (TRM).

An inorganic matrix, at the expense of a slight increase in weight of the structure, has several advantages over an organic one, such as: water-vapour permeability, applicable over a humid substrate, without toxic emissions (special equipment is not needed), cost-effectiveness, high fire-resistance, easy manipulation and application, even to curved surfaces, applicable over irregular deteriorated surfaces, such as a levelling material, without the need for specific treatment, thereby reducing the number of weak joint interfaces, and, finally, no specialized labour is required (Garmendia, 2010).

There are a great variety of textiles to choose for use as a core for the TRM. Experimental results showed that glass fibres, which exhibit weaker mechanical properties than carbon fibres, have strengthened masonry arches more efficiently against collapse mechanisms, and exhibit higher strength and better global ductility (Valluzzi and Modena, 2001). Thus, basalt textiles, which have slightly higher properties than alkali-resistant glass fibres and a much lower cost than carbon or aramid fibres, were applied in this study. This process resulted in Basalt Textile Reinforced Mortar (BTRM).

An in-depth study of compatible and effective strengthening solutions is required, to support the preservation of the valuable cultural heritage of the European Union. Partial results obtained to date with TRM (Papanicolaou et al., 2011; Briccoli Bati et al., 2007) have been satisfactory, but the need to examine the behaviour of this promising reinforcement technology further has been highlighted.

This paper aims, on one hand, to reduce the knowledge gap surrounding the restoration of stone masonry arches and to contribute quantitative results that complement the current database. On the other hand, it endeavours to provide the scientific community with knowledge on the mechanical behaviour of Basalt Textile Reinforced Mortar and to assess its structural effectiveness in different application layouts to arched masonry buildings. Finally, the results will be discussed and compared with those of other authors listed in the bibliography.

2. Material characterisation

2.1. Arches: stone and jointing mortar

Sandstone and poor lime-cement mortar were used for this research, because of their availability and similarity with the masonry works in many historic buildings. The sandstone was quarried at Quintanilla de las Torres (Spain). During the construction of the arches several samples of sandstone and mortar were taken, stored (20ºC and 60%RH) and tested for mechanical characterization according to UNE-EN 1926:2007, UNE-EN 22950-2:1990 for compression (f_{cm}) and indirect tensile (ftm) tests of the stone, UNE-EN1015-11:2000 for compression and flexural (f_{tm}) tests of the mortar and

ASTM C 469:2002 for the elastic moduli (E_{cm}). The average results for both materials are presented in Table 1.

2.2. Strengthening composite material

2.2.1. Matrix mortar

The type and quality of mortar used in the reinforcement are extremely important and crucial to the life of a stone building (Garmendia et al., 2011). Ease of preparation, workability, shrinkage strength, rate of hardening, viscosity and ability to penetrate the textile are the main properties to consider for fresh mortar. On the other hand, with regard to the hardened mortar, moisture and air permeability, compressive and tensile strength, adherence to substrate and textile, ability to tolerate deformation, resistance to outdoor conditions and fire resistance are important properties to take into account.

In this research, the reinforcement was designed with cement-free pozzolanic mortar (MAS, commercial mortar) due to physico-chemical compatibility, which is applied to after a mortar primer (MAR, commercial mortar). MAS mortar has high deformation capacity, a positive point in adapting to the capacity of masonry structures to adjust to deformation. The lack of cement avoids the crystallization of salts, and added to the permeability of the mortar, the preservation of heritage buildings can be promoted. The mortar is modified with polymers in order to improve workability and the adherence between textile and matrix. The results of mechanical tests performed according to the standards mentioned in section 2.1 are show in Table 1.

Table 1. Mechanical properties of the materials

2.2.2. Basalt Textile

Basalt fibres have, in general, excellent alkali resistance, slightly better properties than glass fibres and a considerably lower cost than carbon or aramid fibres. Basalt is roughly 5% denser than glass and its elastic tensile modulus is higher than that of E-glass fibres. The working temperature range is remarkably higher (from -260ºC to 560ºC) compared to that of glass. Moreover, basalt fibres have low elongation ratios and perfectly elastic characteristics up to the point of rupture. These properties result in fabrics with high levels of dimensional stability that exhibit reasonable suppleness, drape ability and good resistance to fatigue. Basalt is non-toxic, completely inert and without any environmental restrictions. Furthermore, basalt fibres show excellent "wet ability" (or natural adhesion) to a broad range of binders, coating compounds and matrix materials in composite applications (García et al., 2012). The manufacturing specifications of basalt textile supplied by FYFE Europe are given in Table 2.

Table 2. Manufacturing specifications of the basalt textile used in this research work.

Figure 1. Pure tensile tests of basalt textile specimens

The textile has been characterised in laboratory by means of uniaxial tensile tests, varying the amount of rovings and testing direction, as presented in Figure 1: one (TL1), two (TL2) and four (TL4) roving specimens were tested in longitudinal directions and four (TT4) roving specimens tested in transversal direction. On the whole, 40 specimens of 400 and 500 mm long were tested in accordance with internal procedure which was based on Standard ASTM D5034, as no explicit regulations or recommendations for testing mineral fibres woven as a mesh are available. The testing machine displacement rate was 5mm/min.

Table 3. Textile tensile test results

Results for the development of deformation and the failure mode are significantly affected by the practical impossibility of providing the same initial length and load to all the fibres. Those that were subjected to greater traction were the first to break.

As presented in Table 3, in the specific case of the TL4, the ultimate resistance (σ_f) is 24% less compared to the ultimate resistance of the specimen with a single strand. This is due to the difficulty of providing the same initial length and load to each one of the thousands of fibre strands that compose the textile and it is aggravated by the higher number of roves. On the other hand, it should be highlighted that failure on specimen type TL4 occurred close to the clamps in the majority of cases, probably due to the stress concentration. Therefore, it can be assumed that the real tensile strength of the specimens is higher than that recorded.

Regarding tensile deformation and the elastic modulus (E_f), the single-strand specimens (TL1) have a higher modulus value, which would imply a more rigid behaviour of the specimens. This can be attributed to the fact that in a single-strand specimen, it is more likely that all the fibres that make it up will be pulled simultaneously. The value of the modulus is slightly lower for the two-strand (TL2) and four-strand (TL4) specimens.

It can also be noticed that the ultimate strength (σ_f) and elastic modulus (E_f) in the transversal direction for four rovings (TT4) is 30% and 18% lower than in the longitudinal direction (TL4), due to the smaller amount of fibres in this direction. The presence of transversal filaments helps to improve fibre-matrix adherence and its adaptation to the form of the structure, but, in this research work, they are not used for absorbing stress in this direction.

2.2.3. Basalt Textile Reinforced Mortar (BTRM)

With the purpose of analysing BTRM tensile behaviour, specimens with cross-sectional area of 100×10 mm^2 and a length of 500 mm were prepared and tested (Figure 2). The specimens were built with one or two layers of basalt textile which was embedded in cement-free MAS mortar (M1 and M2 specimens). These internal layers (800x100mm^2) were positioned in the middle of the cross section and had excess length at each end. Furthermore, so as to promote the failure of the specimen in its middle-third portion, the ends of the specimen were reinforced with two additional textile layers of 200 x 100 mm^2. Slippage between strands and also between the textile and the mortar took place during testing of the M1 type specimens. For this reason, in order to prevent slippage in subsequent tests (M2 type specimens), the gripping device compressed not only the compound material but also the excess textile. After casting, the specimens were kept in a saturated atmosphere for seven days and were then stored for 21 days in a controlled environment (18ºC and 60%RH).

Figure 2. Test set up for pure tensile test of BTRM specimen

The specimens were tested in a universal testing machine and the deformations, within the measurement range, were recorded with four Linear Variable Displacement Transducers (LVDTs), two on each side. The displacement ratio of the test was 0.5 mm/min for M1 specimens and 0.3 mm/min for M2. The tensile test results are presented in Figure 3.

Figure 3. BTRM stress-strain curve for specimen types M1 (left) and M2 (right).

The stress-strain curves (Figure 3) are characterized by the presence of three phases, more defined for M1. In the first phase, Stage I, the specimens showed very rigid behaviour when loads were absorbed with very little deformation; this stiffness reflects the E-modulus of the mortar. This phase ended when the first crack in the mortar appeared and, consequently, the load decreased. The second phase, Stage II, is known as the multiple cracking stage (Hegger et al., 2006). When the mortar tensile strength was exceeded, the first crack formed and the whole tensile force was carried by the textile reinforcement, which had to be able to resist the load acting on the building. Under increased tensile force, new cracks appeared in the specimens. Due to the bond between yarns and mortar, forces were initiated in the matrix, until the tensile strength of the mortar was reached once more and a new crack therefore formed. The distance between cracks and their width is influenced by the reinforcement-matrix bond and the failure strain of the mortar. Stage II ended when no further cracks occurred. This cracking of Stage II causes a delay achieving the ultimate load and increases the deformation capacity which can work as a warning of the load increment. Moreover, it provokes a distribution of forces in the composite material, avoiding stress concentration in certain areas and local damage of the substrate material.

In the third phase, Stage III, the specimen recovered the linear load (with a lower slope than that obtained in Stage I) and only the fibres carried extra load up to the failure point of the composite. The stiffness at this third stage was similar to the elastic modulus of the textile reinforcement (not of the fibres) and its behaviour is basically influenced by the mechanical properties of the textile. The width of the cracks grew due to delamination between fibre and mortar, and led to a loss of the tension stiffening effect. However, the resistance of the transversal fibres meant that the load could continue to increase.

Table 4 presents the numerical results of the tensile tests of the TRM specimens distinguishing the number of layers. E_{TRM} refers to the elastic modulus at Stage III while $e(f_{TRM})$ refers to deformation at the ultimate load.

Table 4. Results of the pure tensile tests of the BTRM specimens

Failure occurred due to rupture of the whole section. While specimens reinforced with one single textile fabric broke smoothly, in the other series the failure was brittle, i.e. an instantaneous loss of bearing capacity. Crack spacing and crack width were dependent on the type and quantity of reinforcement, the bond behaviour between textile and the matrix and the mortar failure strain. The increase of the reinforcement ratio affected the crack pattern (see Figure 4), which strongly influenced the behaviour of the composite: the number of cracks formed was increased and the distance between them was reduced. It was also noted that the increase in the number of layers shortened the length of Stage II. The formation of more cracks favoured the start of the third stage of the curve.

Figure 4. Cracks formed during pure tensile tests of BTRM of M1 (left) and M2 (right) specimens

The value of the Young's modulus in Stage III, in M1 series had a value of 42 GPa, while the value remained almost 42% higher, close to 60GPa in the serie reinforced with two basalt layers. The low amount of internal reinforcement in series M1 can be an explanation of the low values measured.

Finally, in all case, a loss of stiffness prior to the rupture strain can be observed. This effect could be caused by debonding at the interface textile-matrix. A further explanation is the progressive rupture of filaments inside the rovings. When the remaining filaments could not bear the applied load, brittle fracture caused the whole composite to break.

2.3 Physical-chemical analysis of constituent materials compatibility

Regarding the physical-chemical analysis of the sandstone, the petrographic study (see

Figure 5) shows that the rock has fine evenly-sized grains and presents medium to low cohesion and a low degree of compaction. It is composed of 65% quartz in which white grains predominate alongside reddish veins. The sandstone is a uniform, fine-grain, yellowish-grey sandstone rock with light rose-coloured tones, somewhat weak to the touch. The rock could be classified as sub-arkose (Folk, 1974), i.e., a sandstone rock with less that 15% of sandstone matrix, very rich in quartz and with less than 25% of feldspar in the weft.

Figure 5. Microscopic photograph of the sandstone voussoirs

On the other hand, the jointing mortar is made of lime, white cement, sand and water, in volume proportions of 0.5, 2, 10 and 4, respectively. Given that lime mortar takes a lot longer to reach the necessary mechanical strength, in some cases one can speak of centuries, it was considered necessary to add white cement so that the strength of the mortar would increase at an earlier age. It is used to fill the joints and its purpose is to stop the passage of water, regularize the seating between blocks uniformly distributing the load and, finally, to transmit the stress.

The mineralogical analysis of the materials was carried out using the X-ray diffraction technique. The diffractometric measurements were taken using a Philips X'Pert Pro MPD pw3040/60 diffractometer equipped with a copper ceramic tube. The instrument conditions at the time of taking the measurements were continuous 2 to 75° 2 Θ sweep, 40kV, 40 mA generator current for one hour. The analysed sample was ground and homogenized automatically in an MM301Retsch mixing grinder in order to process it adequately. The results are presented in Table 5 and 6. Black dots indicate the relative abundance of the mineral in each specimen.

Table 5. Mineralogical characterization of the stone and jointing mortar

Finally, the strengthening mortars were analysed. The mineralogical analysis of both mortars (base and matrix mortar) is summarised in Table 6.

Table 6. Mineralogical characterization of strengthening mortars

In addition to the mineralogical characterization, the parameters presented in Table 7 were all determined for each material based on current standards: capillarity absorption (UNE-EN 1925:1999 and UNE-EN 1015-18:2003), absorption under atmospheric pressure (UNE-EN 13755:2002), water vapour permeability (UNE-EN 1015-19:1999) and porosity, average pore size and distribution of pore sizes by means of mercury porosimetry (ISO 15901-1:2007).

Table 7. Physical analysis of the materials

This physical-chemical characterization has demonstrated that the stone and the reinforcement mortars have the same stony nature based on silicon arids. Small pores are predominant in the stone, which facilitate absorption by capillarity and decreases the absorption capacity of water at atmospheric pressure. In the base mortar there are two pore sizes, with a higher concentration of the bigger typology. In the matrix mortar, the pore concentration is higher, but its size is smaller than that found in the base mortar. Regarding permeability to water vapour, both mortars have similar magnitude values. Therefore, it becomes evident that the stone is less porous than the reinforcement mortar; the latter allows the flow of humidity through its cavities and stops the accumulation in the interface stone (ashlar stone)-mortar and, therefore, stops the loss of bonding by powdering of the rock or salt-formation phenomenon. That way, compatibility between the reinforcement material and the sandstone is proven on the basis of the hydric properties and, as a consequence, the water-vapour permeability.

3. Arch construction and testing

Eleven stone masonry arches (1.13m span, 0.44m height, 0.25m width, 0.12m thickness, see Figure 6) were erected, strengthened according to different arrangements and tested: two reference arches (R), three strengthened on the extrados (EX), three on the intrados (IN) and three on both sides (EXIN). The main goal was to characterize the structural behaviour of both unstrengthened and strengthened arches and study the effect of the BTRM strengthening system on the mechanical behaviour and failure mechanism depending on the different arrangements. With a view to reproducing the stone arches present in the existing heritage with the highest possible precision, the structures were built by expert builders from the Santa Maria de la Real Foundation, which among its other activities is involved in the restoration of masonry structures, and the constitutive materials are those commonly used in historic Spanish Romanesque masonry structures.

Figure 6. Geometry of the arches.

The reinforcement firstly had a base mortar layer (MAR), to improve adhesion and protect the substrate, on which the matrix mortar was applied (MAS). So as to provide substantial textile thickness, two layers of basalt textile were embedded within the mortar. Furthermore, spike-anchors were used in alternate voussoirs to fix the textile onto the substrate (see Figure 7). They consisted of a threaded basalt yarn inserted into a pre-drilled hole in the stone that is filled with a commercial bi-component epoxy resin. Half of the length of the spike anchor was introduced into the stone, the other half that was outside the stone, helped fix the basalt layers.

Figure 7. Left, numbering of voussoirs and location of spike anchors: a) for arches strengthened on the extrados, b) on the intrados and c) on both surfaces. Right, image of the spike anchors.

An arched masonry structure is stable under a given load condition provided that the thrust line, which represents the internal forces at every cross-section, is kept inside the central core (central third of the thickness). When the thrust line moves outside the central core, the formation and consequent opening of a crack takes place and a plastic hinge is formed. The appearance of successive hinges forms a mechanism that triggers the collapse of the structure (Heyman, 1982). The failure of the arch happens when four hinges are formed.

The strengthening system has as its objective the absorption of the tensile stress that the arch was incapable of bearing beforehand. Thus, the thrust line can lie away from the thickness of the arch, increasing its deformability capacity, but without the formation of hinges. Therefore, in the case of reinforced arches, four new failure mechanisms must be considered: masonry crushing, sliding at the hinges, debonding of the reinforcement due to forces perpendicular to the surface and reinforcement breakage.

Tests were carried out by displacement control applied at the quarter of the span (voussoir number 5, see Figure 6) until failure at a speed of 0.12 mm/min and both horizontal and vertical displacements of alternate voussoirs were recorded during the tests by means of 10 LVDTs. Likewise, displacement outside the vertical plane of the keystone and the stability of the abutments were recorded. Finally, LVDTs were set up to record any possible rotation of the voussoir where the load was applied, in order to monitor the verticality of the applied displacement more closely. In total, 14 displacement meters were used. The applied load was measured using a load cell. Regarding data acquisition, the software MGCplus with an indicator and control panel AB22A/AB32 from HBM was used. Data was recorded at a frequency of 10 Hz. Finally, during the tests, continuous visual inspections were carried out for the control and recording of fissures, formation of hinges, failure modes, etc.

Figure 8 presents the obtained experimental results of every arch up to the failure moment, applied vertical load on voussoir number 5 versus its vertical displacement, in order to analyse its overall structural behaviour.

Figure 8. Vertical load vs displacement of the load application point for each arch.

3.1 Non strengthened arches (R)

Both reference arches R1 and R2 collapsed due to the formation of four hinges that turned the structure into a mechanism. The ultimate loads achieved were 1.3 kN and 1.45 kN, respectively. During the tests, load swings were observed as a result of the settlements of the voussoirs due to irregular crushing of the jointing mortar. Although the order of appearance of the hinges was not the same, their position was identical, except for the hinge that formed on the opposite side of the load, which showed a slight variation (see Figure 10).

3.2 Arches strengthened on the extrados (EX)

In the three cases, the initial structural stiffness was similar. However, starting from an approximate displacement of 6 mm, each of the arches performed in a different way, so a comparison of their structural behaviour is not appropriate. For this reason and from a design point of view, the first peak load was considered to be the ultimate load of the structures: 14.79 kN for the arch EX1; 14.94 kN, EX2 and 12.65 kN, EX3. Arches EX1 and EX2 reached later their maximum load of 19.30 and 16.83 kN respectively (see Figure 8).

It was noted that the strengthening system in arches EX1 and EX2 delayed hinge formation on the intrados of the arch. In the case of EX1, although a sliding at the keystone was also observed, failure was caused by breakage of the BTRM composite in the area under tensile stress, whereas in the case of EX2, the collapse was caused by debonding of the whole BTRM layer. In the case of arch EX3, collapse was caused by the crushing of the voussoir next to the keystone that had been weakened at its source of origin, although it was possible to observe the improvement of the arch's overall strength (see Figure 10).

In EX 2, the anchor placed at voussoir 13 prevented the strengthening strip from debonding as well as at the right abutment where, despite slight delamination, the anchorage maintained the strengthening strip in place until the end of the test. It is worth mentioning that, on the contrary, the anchor embedded at the left abutment was completely extracted, probably because of the normal stress on the surface (produced by the BTRM at its ultimate load stages).

For the sake of simplicity, only load and displacements registered for arch EX1 are shown in Figure 9, where it is corroborated that the displacements correspond with the movements of the structures presented in Figure 10.

Figure 9. Vertical load vs vertical (left) and horizontal (right) displacement in different voussoirs of arch EX1.

3.3 Arches strengthened on the intrados (IN)

With reference to IN1, collapse was due to sliding on the right haunch at an ultimate load of 8.52 kN, which avoided the appearance of the hinge in that area. The collapse of arch IN2 was caused by sliding below load application point, in turn, caused debonding of the strengthening strip at a maximum load of 15.33 kN, and it was not possible to determine the order of appearance of the hinges.

The failure in arch IN2 was characterized by debonding of the strengthening system at the right springer, without tearing off the stone. The absence of an anchor in voussoir 3 (present in the other arches) was verified a posteriori. Due to the high load (15.33 kN) that the structure had to resist at that time (the largest compared to the other two arches), it was not possible to state whether the anchor could have increased the mechanical capacity of the arch.

Arch IN3 reached the failure at a load of 10.07 kN and the failure mode was characterized by debonding of the strengthening strip, which caused all the hinges to appear simultaneously. This debonding was due to the normal thrusts that were generated on the internal surface of the arch. The anchors in the voussoirs located in the area where the strengthening strip became detached appear on the whole to have worked properly, as it was possible to observe strands of the basalt fibre that had broken under traction.

3.4 Arches strengthened on both surfaces (EXIN)

Arch EXIN1 underwent pre-loading, because the first hydraulic cylinder used was not enough to provoke the collapse. Once replaced, the arch reached a maximum load of 28.96 kN, which resulted in debonding of the internal strengthening strip. As from this point, deformation increased considerably, voussoirs 4 and 8 cracked due to the compressive stress and the external strengthening strip located on the right springer nearly separated. Finally, the strengthening BTRM failed due to tensile stresses.

EXIN2 displayed similar behaviour to EXIN1 (slightly stiffer due to the previously discussed pre-load). The structure absorbed the load progressively up until around 20 kN where voussoir 4 cracked. Later on, the load was recovered until the second maximum of 25.5 kN was reached, when debonding of the internal strengthening strip in that area could be observed. The large deformation could be verified, towards the third 25.1 kN load peak, that the arch was experiencing, causing crushing of voussoir 2 and 3. Finally, the load increased until it reached its maximum value (28.3 kN), causing a large deformation of the structure with the rotation of the left springer and its collapse when the external strengthening strip was no longer capable of withstanding the tensile stress in that area.

An exhaustive inspection of the anchors, in those areas where it was possible to do so, clarified that only the anchor located on the internal surface of voussoir 5 was not completely embedded. Nevertheless, debonding of the strengthening strip did not take place in that area.

In arch EXIN3, the first load decrease was due to sliding that took place between voussoirs 6 and 7, which caused debonding of the strengthening strip in the area. As the load recovered, sliding was inhibited due to increased friction. At this stage, the arch underwent considerable deformation. The load was recovered until voussoir 5 crushed under a load of 19.08 kN. Finally, the load was recovered again until its collapse under a maximum load of 21.05 kN, which occurred due to debonding of the internal strengthening strip plus breakage of the external strip at the point where a hinge was formed between voussoirs 11 and 12. Moreover, fractures in voussoirs 7, 11 and 12 were noticed.

4. Discussion of experimental results according to the strengthening arrangement

Figure 10 shows a picture of the failure for every arch in detail, grouped in accordance with the layout of the strengthening strips. Furthermore, the hinges location and order of appearance where possible was presented.

Figure 10. Failure moment for each arch strengthened with different BTRM layouts.

The comparison of the results (Table 8) was carried out only considering the linear behaviour stage of the test and the maximum load applied during the tests. From the first peak load (linear load stage, see Figure 8), every arch is a different structure due to its particular sliding process, hinge formation history, etc., a comparison of its behaviour with other arches not being strictly possible.

Table 8. Summary of the experimental tests results

In the case of the non-strengthened arches, it may be clearly observed that the failure mode is characterized by the formation of four hinges that cause the structure to turn into a mechanism under an average ultimate load of 1.38 kN and a limited displacement capacity of voussoirs (1.43 mm for the load application point).

In the case of the arches strengthened on their external surfaces, no one single failure pattern was shown. Moreover, no relevant conclusion could be obtained from EX3 as it was weakened at its source of origin. Experimental data showed a considerable increase in the mechanical capacity with an average linear load value of 14.12 kN, 10.23 times larger compared to the non-strengthened arches. Likewise, a higher degree of structural ductility was observed. If the maximum load obtained is considered, the average value is 16.26 kN, 11.78 larger than non-strengthened arches and displacement is 6.14 times higher.

The arches strengthened on the intrados were, on the contrary, characterized by a linear behaviour where failure took place, due to debonding of the strengthening system or sliding between the voussoirs, which caused the debonding in specific cases, due to normal stresses on the internal surface. These facts limited the deformation capacity of the structure while the bearing load was 8.20 higher than non-strengthened arches, at an average value of 11.31 kN.

Finally, the arches strengthened on both surfaces failed due to voussoir crushing and debonding of the internal strengthening strip. The former took place at around 20 kN while the latter occurred around 25 kN. When subjected to a large increase in the load, the mechanical properties of the stone became the weakest point of the structure. The average ultimate load obtained with this strengthening arrangement was 19.23 kN, almost 14 times higher than non-strengthened arches. This value is affected by the result considered for EXIN3 which showed a more ductile behaviour, with a lower bearing capacity, due to the sliding occurred in a joint. If there had been no slippage, the ultimate load would have been 19.08 kN (where material crushing happened) and the average ultimate load 23.04 kN, 16.70 times greater than non-strengthened arches. Considering the maximum loads, the average load obtained was 26.1 kN, 18.91 times larger than the reference arches.

In all test cases, the debonding of the strengthening strip took place cleanly, which is to say that there was no ripping of the stone, which helps the preservation of the structures, a very important factor for heritage buildings in line with the initial comments from the author about the compatible nature of the TRM strengthening technique.

On the other hand, the effect of the spike anchors was very difficult to study. The structures apparently remained unaltered up to the point where the hinges started to form, for which reason it was not possible to deduce visually whether the anchors had a valuable effect. It seems that anchors, if well executed, should contribute to keeping the strengthening strip bonded to the surface, helped, in turn, by adhesion between the strengthening strip and the support. In any case, in view of the other results, it can be concluded that spike anchors avoided slipping of the strengthening system which leads to a more ductile failure.

5. Comparison with results obtained by other authors

With reference to results obtained by other authors, due to variations in materials, geometries, strengthening systems and test methodologies, any rigorous comparison with the results provided in this research work is a complex task. Nevertheless, within an overall comparison framework, Table 9 lists the results of experimental work on arches/vaults made from ceramic masonry recorded in different research works. The strengthening materials used were FRP, SRG (Steel Reinforced Grout) or TRM in different layouts. The aim is to analyse which strengthening arrangement gives place to the highest mechanical capacity and the failure mode that provokes; Highest Ultimate Load and Highest Deformability refer to the strengthening arrangement that occasioned the highest value of load and deformability, respectively. When a unique strengthening arrangement was used, these columns are left in blank. The strengthening was never applied in both surfaces. Failure Mode presents what provoked the failure for each arrangement.

Table 9. Comparison of results from different authors

As presented in Table 9, regardless of the strengthening composite material, for arches strengthened on the extrados, failure is mainly due to sliding (except for Cancelliere et al, and the results of this work, in both cases strengthened arches are of similar geometric characteristics), while for arches strengthened on the intrados, debonding of the strengthening strip is the main reason for collapse, although there is no unique failure mode, as sliding and composite rupture are also registered. Furthermore, in most of the literature, arches strengthened on the extrados possess greater ductility.

Finally, in the same way as presented by Briccoli Bati (2007), Jasienko (2009), Carbone (2010), the results obtained in this work show that reinforcement based on inorganic matrices prevent the substrate from tearing off, which is common in polymer-based reinforcements. This is a very important property for the preservation of historical heritage.

6. Conclusions

The building and subsequent testing of eleven shallow stone masonry arches non-strengthened and strengthened with Basalt Textile Reinforced Mortar according to certain layouts confirmed the effectiveness of this cost effective strengthening system, the simplicity of its application, (mainly based on traditional techniques) and the adaptability to curve surfaces. The cement-free mortars used provide physical-chemical compatibility with the stone substrate and, another key issue of the inorganic matrix base composite is that the failure mode does not include delamination of the masonry (this aspect has also been detected in bibliography). These two aspects are important to safeguard the aesthetics of historic buildings and confirm its cultural compatibility with this structural typology.

The increase in the ultimate load and deformability of the strengthened structures was significant in all cases, as the appearance of hinges that provoke a mechanism is postponed. The selection of the best arrangement to use will depend on the possibility of being able to execute it (accessibility, aesthetic, etc.) and the desired solution.

According to the results obtained in this research and those presented in other works, the different strengthening layouts vary in effectiveness and each one has advantages and disadvantages. There is no an agreement about which strengthening arrangement resists the highest ultimate load or has the highest deformation capacity.

Acknowledgements

This research work has been made possible thanks to financing from the Basque Government (TEXMOR-S-PE07LA09) and the Diputación Foral de Bizkaia (BIRGAITEK 7-12-TK-2009-10).

References

ASTM C 469:2002: Standard test method for static modulus of elasticity and Poisson's ratio of concrete in compression.

ASTM D5034-09: Standard Test Method for Breaking Strength and Elongation of Textile Fabrics (Grab Test).

Baratta A. and Corbi O. 2007. Stress analysis of masonry vaults and static efficacy of FRP repairs. *International Journal of Solids and Structures,* 44(24):8028–8056.

Basilio I. 2007. Strengthening of arched masonry structures with composite materials. *PhD Thesis.* Escola de Engenharia Universidade do Minho.

Borri A., Casadei P., Castori G. and Ebaugh S. 2007. Research on composite strengthening of masonry arches. *FRPRCS-8*. ISBN 978-960-89691-0-0.

Briccoli Bati S. and Rovero L. 2008. Towards a methodology for estimating strength and collapse mechanism in masonry arches strengthened with fibre reinforced polymer applied on external surfaces. *Materials and Structures*. 41(7):1291–1306.

Briccoli Bati S., Rovero L., Tonietti U. 2007. Strengthening masonry arches with composte materials. *Journal of Composites for Construction*, 11(1):33-41.

Cancelliere I., Imbimbo M. and Sacco E. 2010. Experimental tests and numerical modeling of reinforced masonry arches. *Engineering Structures,* 32:776-792.

Carbone I. 2010. Delaminazione di compositi a matrice cementizia su supporti murari. *Doctoral Thesis.* Universitá degli studi Roma Tre.

Croci G., Ayala D., Asdia P. and Palombini F. 1987. Analysis on shear walls reinforced with fibres. *IABSE Symp. on Safety and Quality Assurance of Civil Engineering Structures*, Tokyo, Japan.

Folk, R.L. *Petrology of Sedimentary Rocks*. 1974, Hemphills, Texas, USA.

Foraboschi P. 2001. Strengthening of masonry arch bridges using advanced composite materials. *Composites in Construction*. ISBN 90-2651-858-7.

Foraboschi P. 2004. Strengthening of masonry arches with Fiber-Reinforced Polymer Strips*. J. Compos. Constr*. 8: 191-202.

García D., San-José J.T., Garmendia L., San-Mateos R. 2012. Experimental study of traditional stone masonry under compressive load and comparison of results with design codes. *Materials and Structures* 45(7):995–1006.

Garmendia L. 2010. Rehabilitation of masonry arches by a compatible and minimally invasive strengthening system. *Doctoral Thesis*. Escuela de Ingeniería de Bilbao (UPV/EHU).

Garmendia L., San-José J.T., García D. and Larrinaga P. 2011. Rehabilitation of masonry arches with compatible advanced composite material. *Construction and Building Materials,* 25:4374-4385.

Hegger J, Will N, Bentur A, Curbach M, Jesse F, Mobasher B, Peled A, Wastiels J. 2006. Mechanical Behaviour of Textile Reinforced Concrete. Textile Reinforced Concrete. *State-of-the-Art Report of RILEM Technical Committee 201-TRC*. Ed. Brameshuber W. ISBN:2- 912143-99-3. pp. 135.

Herrera L.K., Le Borgne S. Videla H.A. 2009. Modern methods for materials characterization and surface analysis to study the effects of biodeterioration and weathering on buildings of cultural heritage. *International Journal of Architectural Heritage* 3:74-91.

Heyman J. 1982. *The masonry arch.* Ellis Horwood Limited.

ISO 15901-1:2007

Jasienko J., Di Tommaso A. and Lukasz B. 2009. Experimental Investigations into Collapse of Masonry Arches Reinforced Using Different Compatible Technologies. *MuRiCo3 Conference, Meccanica delle strutture in muratura rinforzate con compositi*. 22-24, Venice.

Jerez E., León J., Martín-Caro J.A. 2007. *Insp*ección y diagnosis de puentes ferroviarios de fábrica. *Adif.*

Lissel S. L. and Gayevoy A. 2003. The use of FRP's in masonry: A state of the art review. *In Proc. International Conference on the Performance of Construction Materials*, Cairo, Egypt; pp. 1243–1252.

Oliveira D., Basilio I. and Lourenço P. 2006. FRP strengthening of masonry arches towards an enhanced behaviour. *Bridge maintenance, safety, Management, Life Cycle Performance and Cost.* Cruz, Frangopol & Neves (eds) Taylor & Francis Group, London, ISBN 0415403154.

Oliveira D. V., Lourenço P.B., Lemos C. 2010. Geometric issues and ultimate load capacity of masonry arch bridges from the northwest Iberian Peninsula. *Engineering Structures*, 32 (12)::3955-3965.

Orban Z. 2007. UIC Project on assessment, inspection and maintenance of masonry arch railway bridges*.ARCH'07 – 5th International Conference on Arch Bridges*. September 12-14, Madeira, Portugal.

Papanicolaou C. Triantafillou T., Lekka M. 2011. Externally bonded grids as strengthening and seismic retrofitting materials of masonry panels. *Construction and Building Materials* 25(2): 504–514.

Seible F. 1995. Repair and seismic retest of a full-scale reinforced masonry building. *Proceedings of the 6th International Conference on Structural Faults and Repair*. Vol. 3, 229-236.

Tao Y., Stratford T.J., Chen J.F. 2011. Behaviour of a masonry arch bridge repaired using fibre-reinforced polymer composites. *Engineering Structures,*33:1594–1606.

Triantafillou T.C. 1996. Innovative strengthening of masonry monuments with composites. *Proceedings of 2nd International Conference Advanced Composite Materials in Bridges and Structures*, Montreal, Quebec, Canada.

UNE-EN 1015-11:2000. Methods of test for mortar for masonry. Part 11: Determination of flexural and compressive strength of hardened mortar.

UNE-EN 1015-18:2003. Methods of test for mortar for masonry. Part 18 : Determination of water absorption coefficient due to capillary action of hardened mortar.

UNE-EN 1015-19:1999. Methods of test for mortar for masonry. Part 19: Determination of water vapour permeability of hardened rendering and plastering mortar.

UNE-EN 1925:1999. Natural stone test mehods. Determination of water absorption coefficient by capillarity.

UNE-EN 1926:2007. Natural stone test methods. Determination of uniaxial compressive strength.

UNE 13755:2002

UNE-EN 22950-2:1990. Mechanical properties of rocks. Strength determination tests. Part 2: Traction strength. Indirect determination. (Brazilian Test).

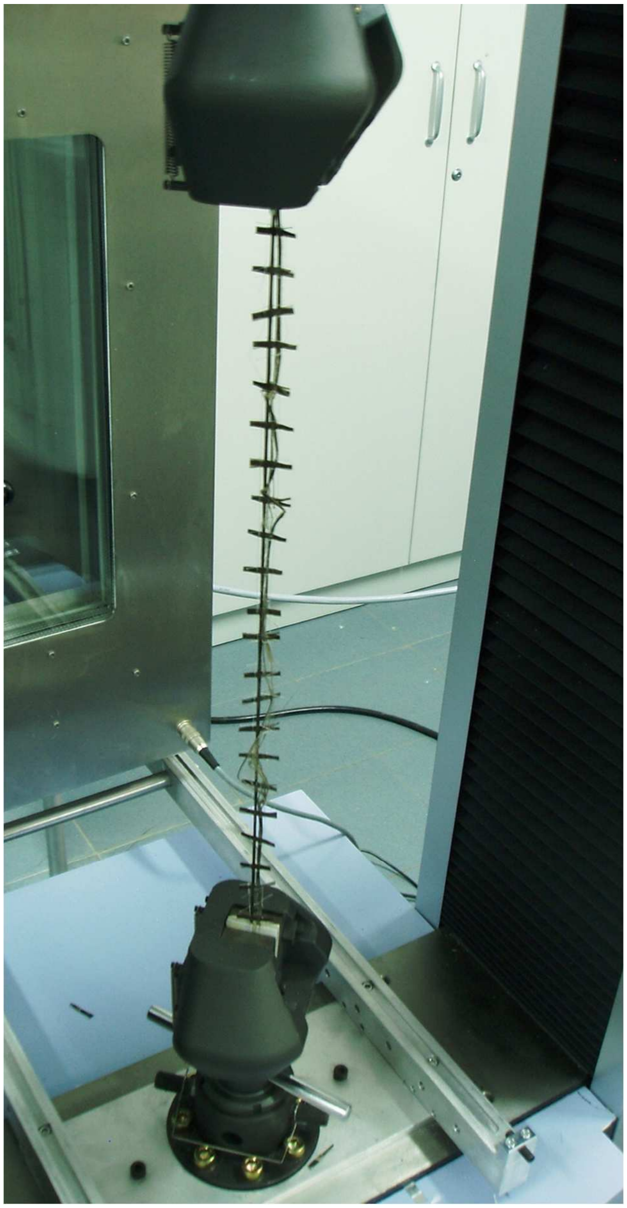

Pure tensile tests of basalt textile specimens
70x135mm (300 x 300 DPI)

Test set up for pure tensile test of BTRM specimen
70x139mm (300 x 300 DPI)

BTRM stress-strain curve for specimen types M1 (left) and M2 (right).
70x125mm (300 x 300 DPI)

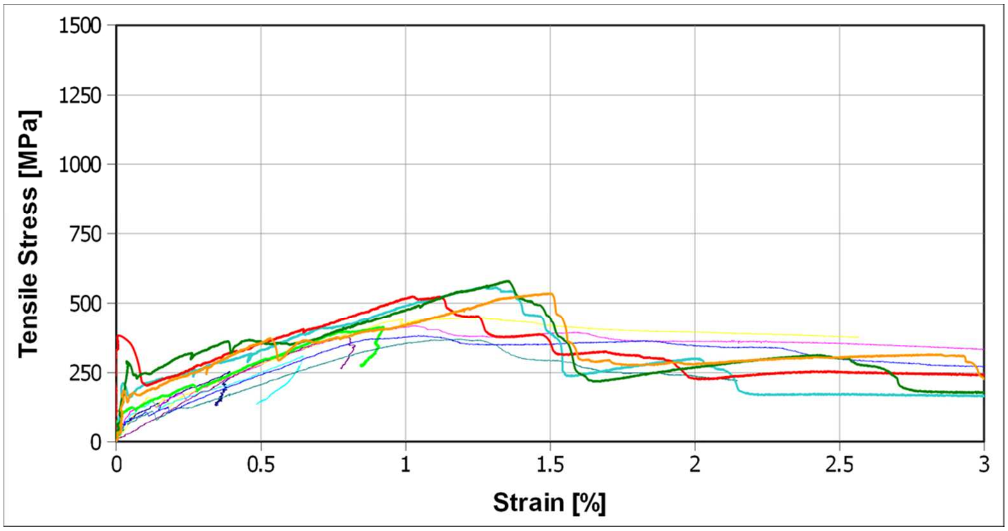

BTRM stress-strain curve for specimen types M1 (left) and M2 (right).
99x52mm (300 x 300 DPI)

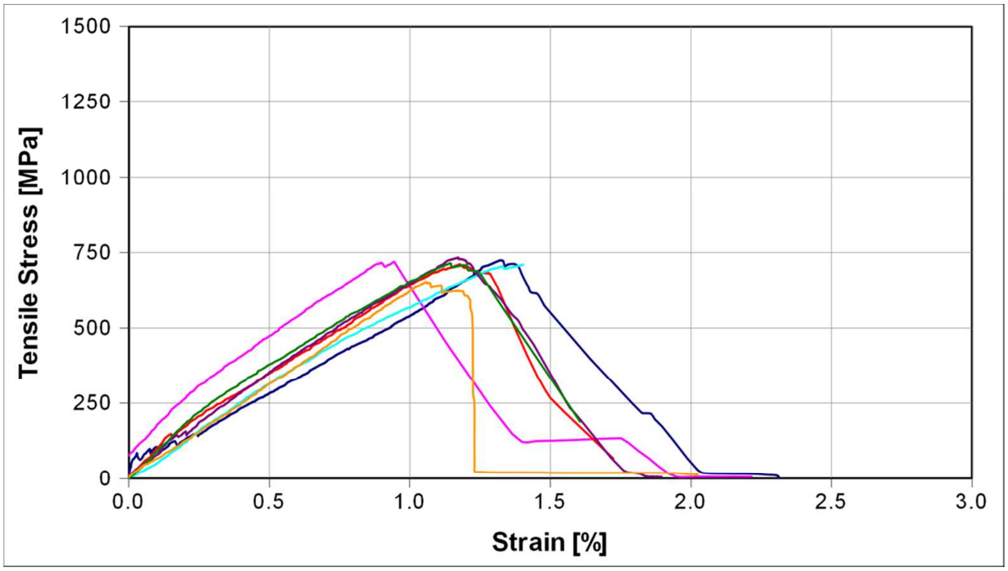

BTRM stress-strain curve for specimen types M1 (left) and M2 (right).
99x56mm (300 x 300 DPI)

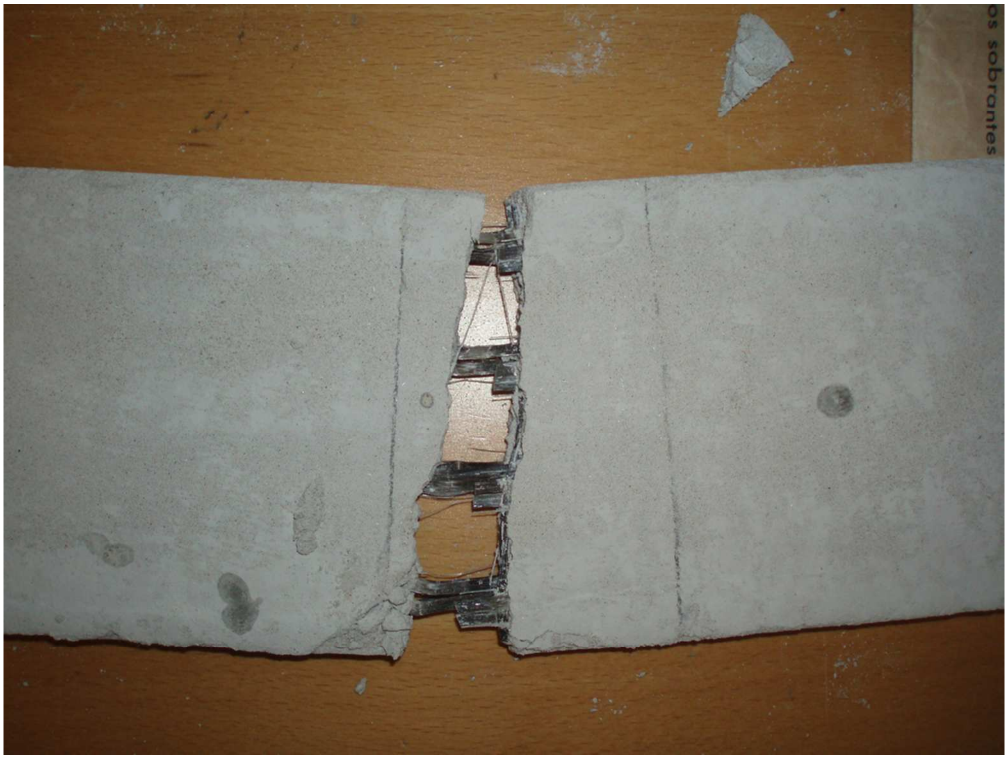

Cracks formed during pure tensile tests of BTRM of M1 (left) and M2 (right) specimens
99x75mm (300 x 300 DPI)

Cracks formed during pure tensile tests of BTRM of M1 (left) and M2 (right) specimens
99x79mm (300 x 300 DPI)

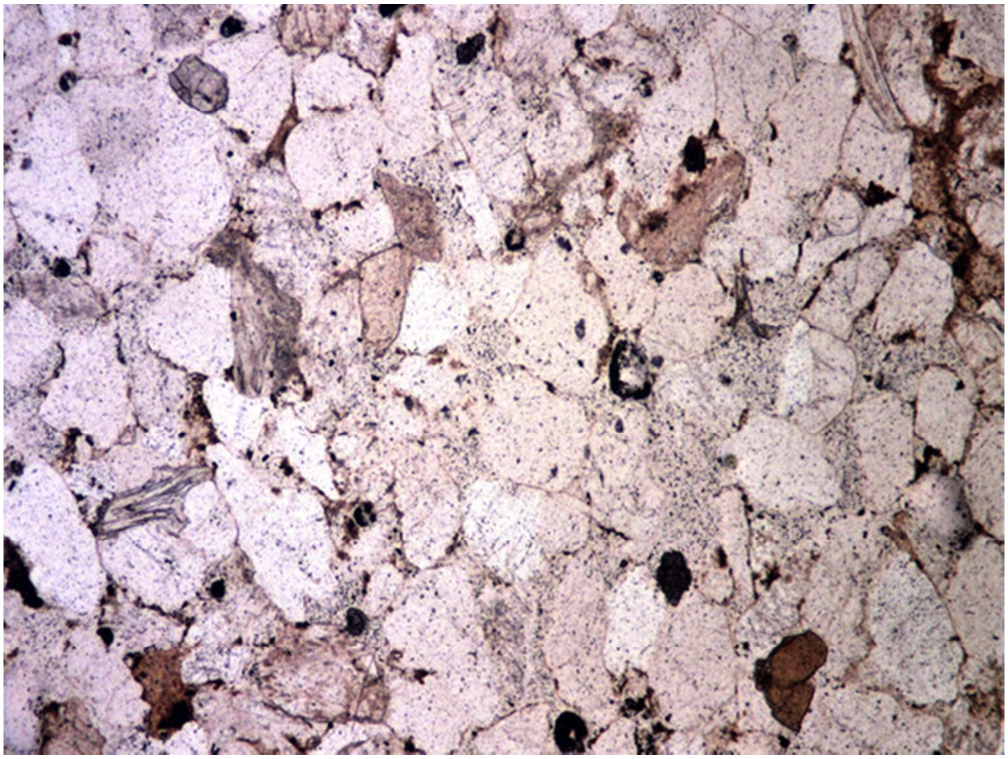

Microscopic photograph of the sandstone voussoirs
48x36mm (300 x 300 DPI)

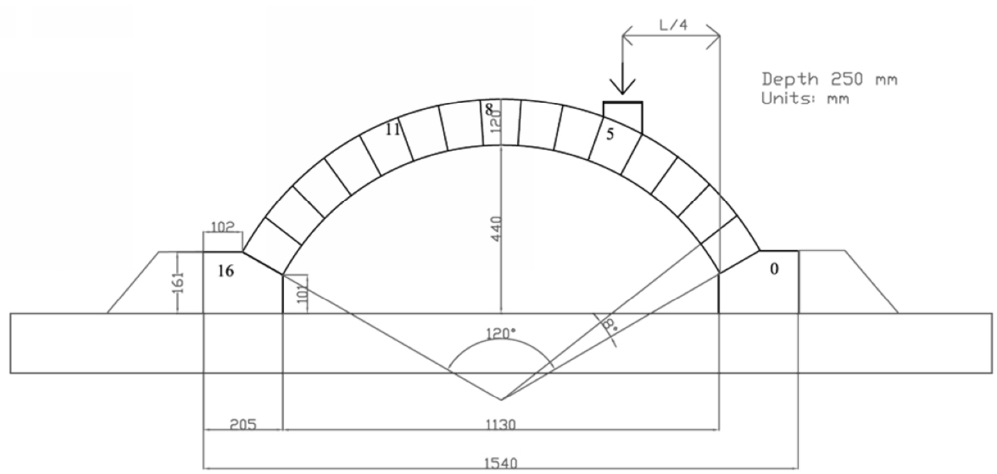

Geometry of the arches
312x152mm (96 x 96 DPI)

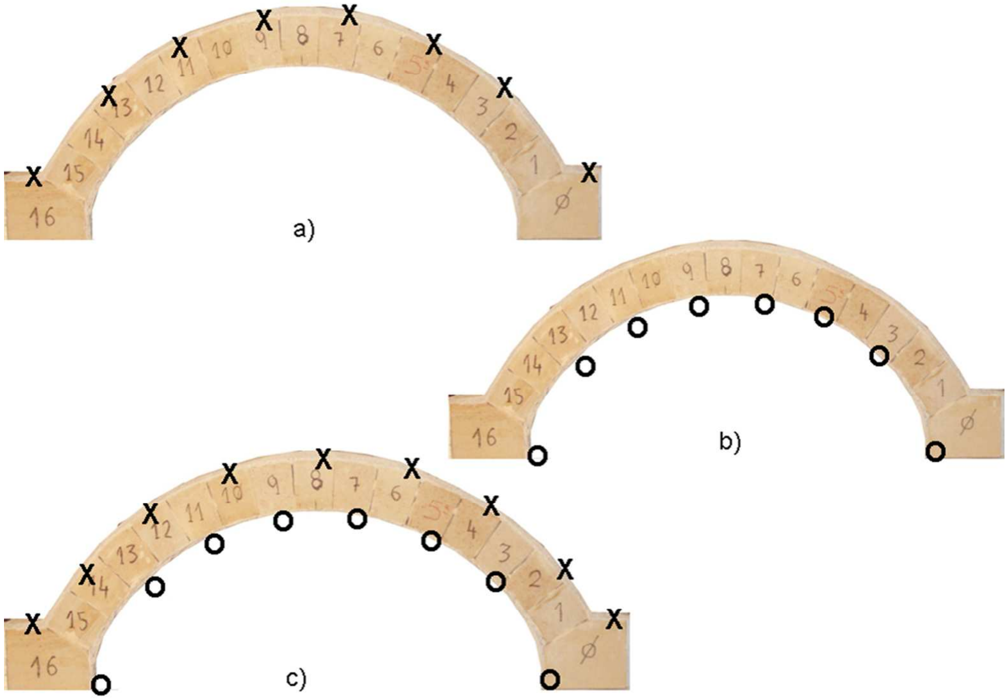

Left, numbering of voussoirs and location of spike anchors: a) for arches strengthened on the extrados, b) on the intrados and c) on both surfaces. Right, image of the spike anchors.
81x60mm (300 x 300 DPI)

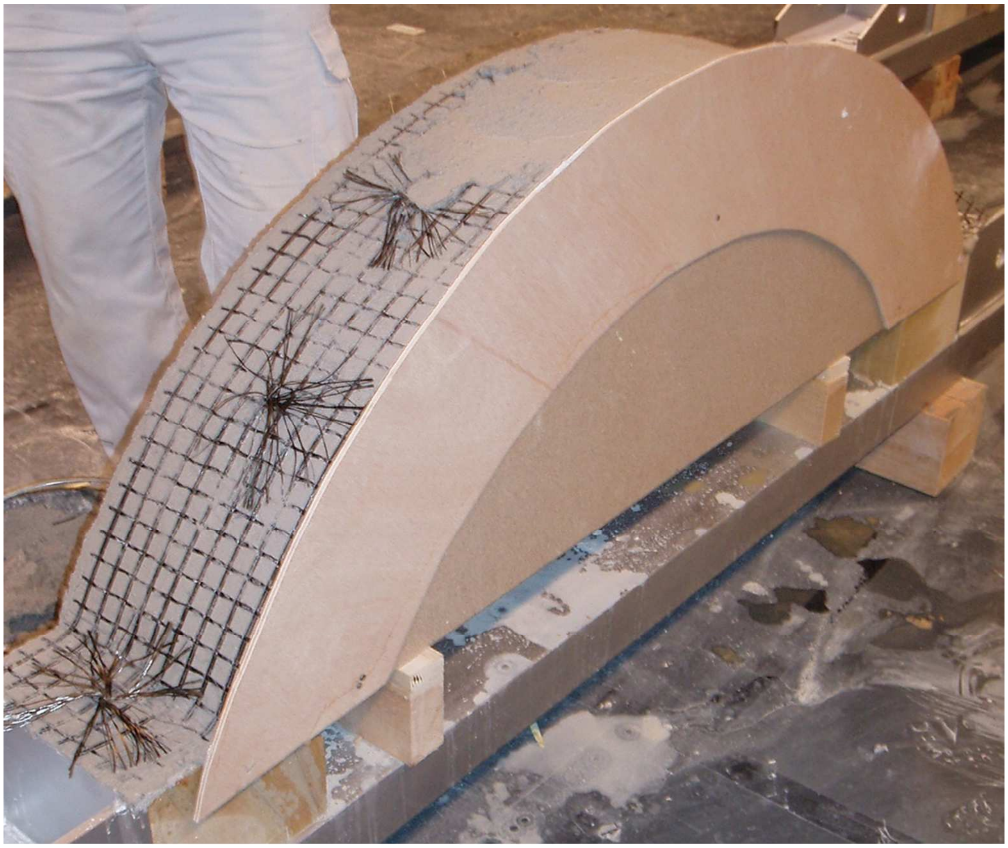

Left, numbering of voussoirs and location of spike anchors: a) for arches strengthened on the extrados, b) on the intrados and c) on both surfaces. Right, image of the spike anchors.
99x83mm (300 x 300 DPI)

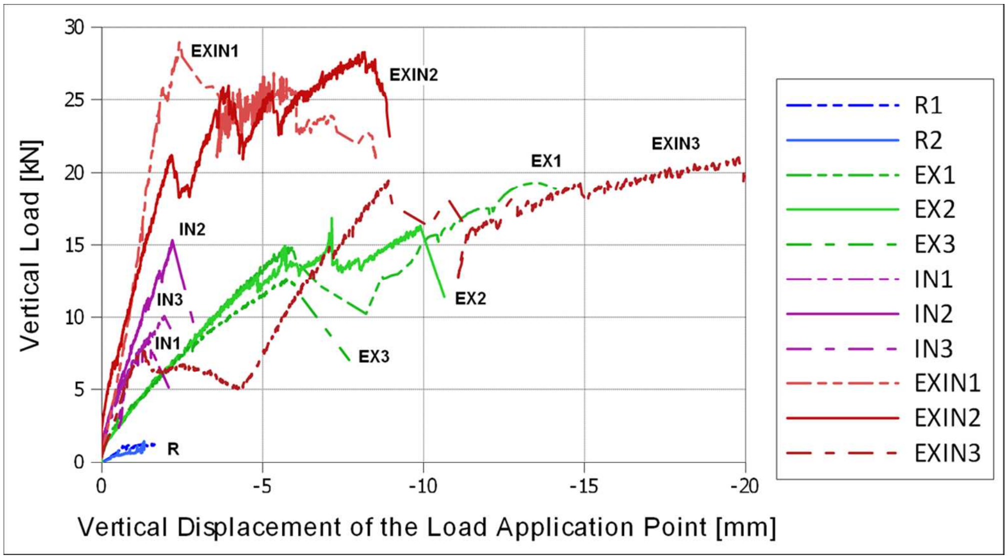

Vertical load vs displacement of the load application point for each arch.
109x60mm (300 x 300 DPI)

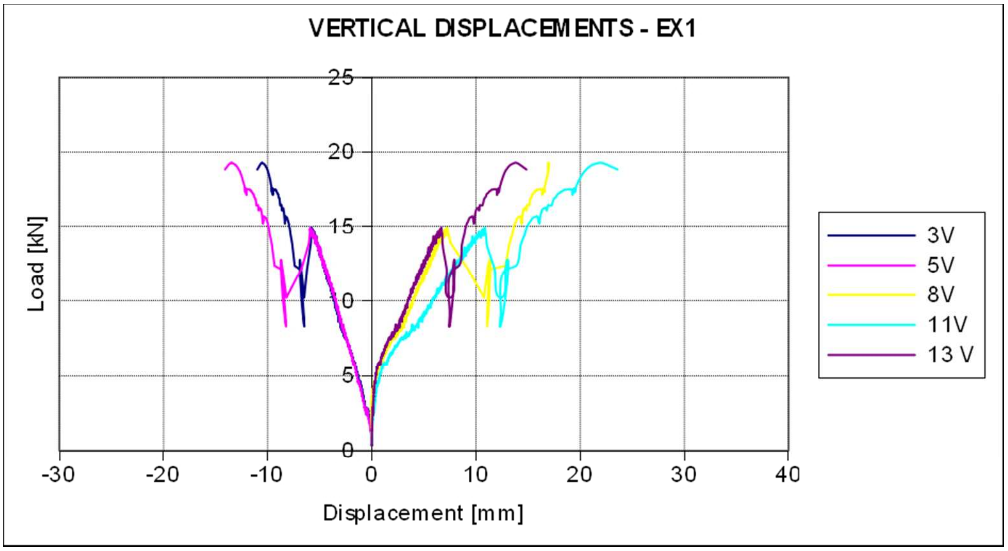

Vertical load vs vertical (left) and horizontal (right) displacement in different voussoirs of arch EX1
79x43mm (300 x 300 DPI)

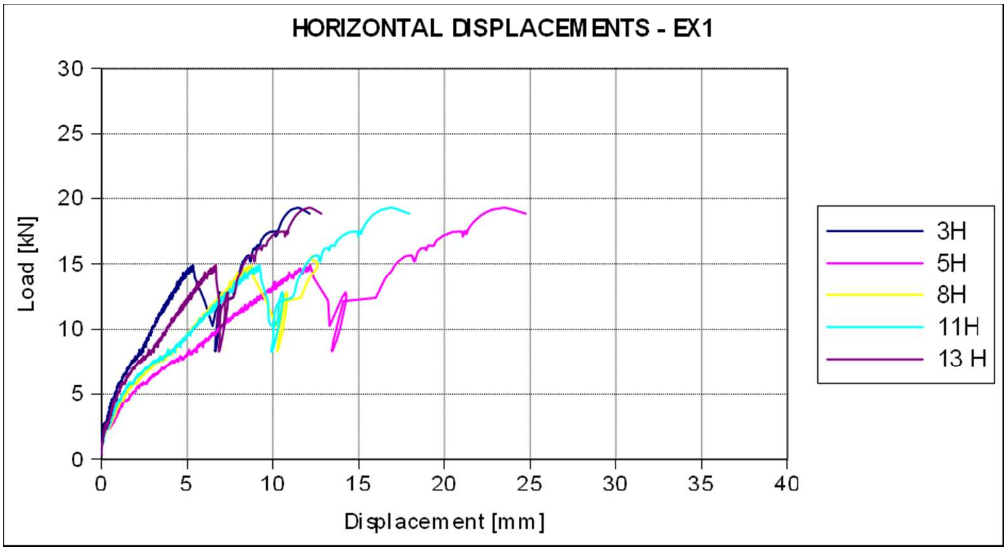

Vertical load vs vertical (left) and horizontal (right) displacement in different voussoirs of arch EX1
79x43mm (300 x 300 DPI)

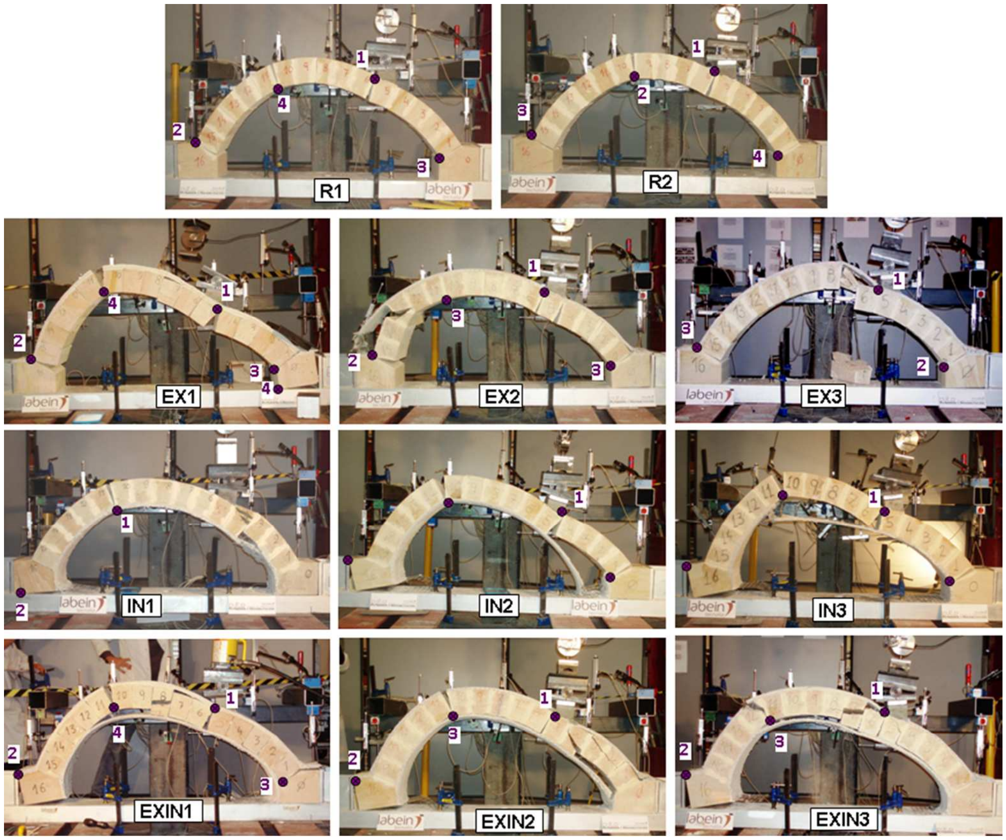

Failure moment for each arch strengthened with different BTRM layouts
73x60mm (300 x 300 DPI)

Table 1. Mechanical properties of the materials

	f_{cm} *[MPa]*	f_{tm} *[MPa]*	E_{cm} *[GPa]*
Sandstone	21.3	1.36	5.9
Jointing Mortar	2.03	0.98	5.0
MAR Mortar	12.6	1.9	7.2
MAS Mortar	21.6	3.5	15.7

Table 2. Manufacturing specifications of the basalt textile used in this research work.

Density by area[a]	233 g/m^2
Side length of cell	25 mm
Average thickness: Uniaxial tension[b]	0.0424 mm
Biaxial tension[c]	0.0848 mm
Elastic modulus of the fibre	89 GPa

[a] Density expressed without considering the bitumen that impregnates the basalt fibres
[b] $t = 0.5\ M / \rho = 0.5 * 233\ [g/m^2] / 2.750\ [kg/m^3] = 0.0424$ mm
[c] $t = M / \rho = 233\ [g/m^2] / 2.750\ [kg/m^3] = 0.0848$ mm

Table 3. Textile tensile test results

Specimen type	f_f [N]	σ_f [MPa]	f_f [mN/Tex]	$e(f_f)$	E_f [GPa]
TL1	1240	1170	417	0.0224	56
TL2	2693	1270	453	0.0292	49
TL4	3790	894	319	0.0218	52
TT4	2849	671	240	0.0238	43

Force per linear density expressed as mN/tex is used in industry specifications of fibre textiles. It represents the milli-Newtons supported by the weight in grams of 1,000 metres of the fibre yarn
Tensile results were obtained for an equivalent section of 1.06 mm2 per strand.

Table 4. Results of the pure tensile tests of the BTRM specimens

Specimen	Nº of plies	f_{TRM} [N]	σ_{TRM} [MPa]	$e(f_{TRM})$	E_{TRM} [GPa]
M1	1	1897	447	0.0121	42
M2	2	6015	711	0.0118	57

Table 5. Mineralogical characterization of the stone and jointing mortar

Mineral Phase		Specimen	
		Stone	Jointing Mortar
Calcite	$CaCO_3$		••
Kaolinite	$Al_2Si_2O_5(OH)_4$	•	
Quartz	SiO_2	•••••	•••••
Potassium feldspar (Microcline)	$KAlSi_3O_8$	••	••
Portlandite	$Ca(OH)_2$		••
Muscovite	$KAl_2(AlSi_3O_{10})(OH)_2$	••	•
Gypsum	$CaSO_4*H_2O$		•
Ettringite	$Ca_6Al_2(SO_4)_3(OH)_{12}*26H_2O$		•

Table 6. Mineralogical characterization of strengthening mortars

Mineral Phase		Specimen			
		MAR		MAS	
		Material powder form	Hardened specimen	Material powder form	Hardened specimen
Calcite	$CaCO_3$	●●	●●	●●●●	●●●●●
Quartz	SiO_2	●●●●●	●●●●●	●●●●●	●●●●
Epidote	$Ca_2FeAl_2Si_3O_{12}(OH)$		●		
Ettringite	$Ca_6Al_2(SO_4)_3(OH)_{12}*26H_2O$				●
Potassium feldspar (Microcline)	$KAlSi_3O_8$	●●	●	●●	●
Sodium Feldspar (albite)	$NaAlSi_3O_8$	●●	●●	●●	●
Portlandite	$Ca(OH)_2$	●●	●●		
Gypsum	$CaSO_4*H_2O$			●	
Zeolite (gismondite)	$CaAl_2Si_2O_8*4H_2O$	●●	●●		

Table 7. Physical analysis of the materials

Mortar type	Density [Kg/m^3]	Capillarity absorption [Kg/m^2 min-$^{1/2}$]	Absorption under atmospheric pressure %	Water vapour permeability [Kg/m s Pa]	Porosity %	Average pore size Ø [µm]	Pore size distribution
Sandstone	2011	1.48	6.5	-	20.4	28	Unimodal with asymmetry (lowest values)
Jointing Mortar	1625	1.74	-	-	34.1	-	
MAR	1880	0.18	11.69	2.97E-12	26.44	0.05	Bimodal. Two-pore families. Average size of 0.75 and 0.04 µm.
MAS	2060	0.36	15.79	2.07E-12	29.92	0.04	Unimodal.

Table 8. Summary of the experimental tests results

	Linear Load				Maximum Load				
Arch type	Linear Load [kN]	Average / Increment [kN] / [-]	Displacement [mm]	Average / Increment [mm] / [-]	Maximum Load [kN]	Average / Increment [kN] / [-]	Displacement [mm]	Average / Increment [mm] / [-]	Failure Mode
R1	1.30	1.38	1.56	1.43	-	-	-	-	Mechanism
R2	1.45		1.30						Mechanism
EX1	14.79		5.93		19.30		13.5		Sliding in a joint
EX2	14.94	14.12 / x 10.23	5.69	5.81 / x 4.06	16.83	16.26 / x 11.78	7.14	8.79 / x 6.14	BTRM debonding
EX3	12.65		5.81		12.65		-		Masonry crushing
IN1	8.52		1.41						Sliding in a joint
IN2	15.33	11.31 / x 8.20	2.19	1.84 / x 1.29	-	-	-	-	Sliding in a joint
IN3	10.07		1.94						BTRM debonding
EXIN1	28.96		2.41		28.96		-		BTRM debonding
EXIN2	21.10	19.23* / x 13.93	2.12	1.92 / x 1.34	28.30	26.1 / x 18.91	8.16	10.12 / x 7.08	Masonry crushing
EXIN3	7.63		1.22		21.05		19.80		Sliding in a joint

(*) Penalized by the behaviour of EXIN3 (-) when the maximum values were obtained in the linear area.
Displacement refers to the vertical displacement of the load application voussoir and *Increment* is obtained with respect to reference arches.

I

Table 9. Comparison of results from different authors

AuthoReferences	Strengthening material	Highest Ultimate Load	Highest Deformability	Failure Mode
Valluzzi and Modena, 2001	FRP	EX	EX	EX: sliding IN: debonding
Basilio, 2007	FRP	IN	EX	EX: sliding IN: debonding
Foraboschi, 2004	FRP	IN	IN	EX: sliding IN: debonding
Baratta and Corbi, 2007	FRP	IN	EX	EX: sliding IN: debonding
Briccoli Bati and Rovero, 2008	FRP	EX	EX	EX: sliding IN: debonding
Jasienko et al., 2009	FRP			EX: sliding
Cancelliere et al., 2010	FRP			EX: material crushing
Tao et al., 2011	FRP			IN: debonding
Borri et al., 2007	FRP	IN	EX	EX: sliding IN: TRM rupture
Borri et al., 2007	SRG	-	EX	EX: sliding IN: TRM rupture / debonding
Jasienko et al., 2009	TRM			EX: sliding
Present work	TRM	EX	EX	EX: sliding / debonding IN: sliding / debonding:

EX: arch strengthened on the extrados

IN: arch strengthened on the intrados

(-) Unavailable results